Coarse-Grained Model Simulations of Mixed-Lipid Systems: Composition and Line Tension of a Stabilized Bilayer Edge

Jason de Joannis, Frank Y. Jiang, and James T. Kindt*

Department of Chemistry and Emerson Center for Scientific Computation, Emory University, Atlanta, Georgia 30322

Received May 13, 2005. In Final Form: October 14, 2005

Bilayer disks and ribbons composed of a mixture of short- and long- tail phospholipids have been studied by molecular dynamics with a coarse-grained model. The effects of system composition on the edge structure, composition, and line tension were analyzed. Increases in the fraction of short-tail lipids tend to decrease the line tension (i.e., stabilize the edge) but not eliminate it. The short-tail lipid is generally enriched at the curved rim forming the bilayer edge, with an excess of 3 to 4 molecules per nanometer (relative to the bulk), but complete segregation was not observed. In all mixtures, a region depleted in the short-tail component occurs just before the edge, corresponding to a bulge in the bilayer thickness. The bulge and depletion are more prominent as the bilayer composition shifts toward a majority of short-tail lipids. In one case, a net excess of long-tail lipids at the edge was demonstrated, suggesting that certain circumstances give rise to a "segregation inversion" in which the long-tail lipid behaves as an edge stabilizer.

1. Introduction

The properties of lipid bilayers are of practical interest for their utility (in nature and in encapsulation technologies) as self-assembled, semipermeable, flexible membranes that can compartmentalize small volumes in aqueous systems. The statistical thermodynamics of bilayers has been a rich area of activity for theory and simulation through models of varying degrees of detail, from the atomistic[1−3] through coarse-grained molecular models[4,5] to mesoscale representations of the bilayer as a triangulated surface or elastic continuum.[6,7] One source of the bilayer's utility is its mechanical strength, which can be related to the line tension of the bilayer edge—the reversible work required to create a unit length of free edge from an intact membrane. The line tensions of membranes formed from biologically important lipids are typically on the order of 10 pN[8] ($\sim^1/_4 k_B T$/Å), great enough that free edges tend to be observed only as unstable transient structures. Certain amphiphilic molecules, however, are known to behave as edge-active agents ("edgactants") that reduce this line tension or even eliminate it altogether to allow stable aggregate structures with edges such as pores[8] or disks.[9] The most widely studied system with stabilized edges is a mixture of the common bilayer-forming glycerophospholipid dimyristoyl phosphatidylcholine (DMPC) and its analogue dihexanoyl phosphatidylcholine (DHPC). The two have identical zwitterionic headgroups but different length alkyl tails of C14 and C6, respectively. Aggregates formed from this mixture have been used as an alignable medium in numerous NMR studies on membrane−protein structures.[10] Originally, DMPC/DHPC mixtures were proposed to form disk-shaped aggregates, termed "bicelles", for bilayered micelles over a wide range of the lipid ratio, temperature, concentration, and pH.[11] (Some discrepancies appear in the literature on the use of the term "bicelle". Throughout this article, we apply it only to disk-shaped aggregates.) In a simplified representation called the "ideal bicelle," a circular bilayer interior composed entirely of DMPC is capped by a rounded edge formed from DHPC molecules; the size of the bicelle therefore depends only on the ratio of these two lipids. Although it is widely agreed that small isotropic disks form for DMPC/DHPC ratios near or below 1:1 and temperatures below the DMPC melting transition,[10,12,13] recently alternative structures have been proposed for higher temperatures, DMPC ratios, and lipid concentrations. The original argument invoked in the alignable disk hypothesis was derived from the separation in NMR resonances corresponding to ordered DMPC molecules and disordered DHPC molecules.[14] However, this observation is also consistent with perforated bilayer lamellae.[10,15−18] Other interesting structures include wormlike micelles,[10,19] wormlike networks,[10] ribbons,[19] and perforated vesicles.[16,20] The predominance of the disk morphology has also been questioned from a theoretical model that considers elastic and entropic effects.[21] The other conventional assumption that complete segregation of DMPC into bilayers and DHPC into edges occurs has also been questioned.[10,20] The "mixed bicelle" was introduced to better explain the existing body of data that allows a residual of DMPC at the edge and a noncircular cross section for the rim.[20] Molecular

(1) Saiz, L.; Klein, M. L. *Acc. Chem. Res.* **2002**, *35*, 482−489.
(2) Scott, H. L. *Curr. Opin. Struct. Biol.* **2002**, *12*, 495−502.
(3) Norberg, J.; Nilsson, L. *Q. Rev. Biophys.* **2003**, *36*, 257−306.
(4) Müller, M.; Katsov, K.; Schick, M. *J. Polym. Sci., Part B* **2003**, *41*, 1441−1450.
(5) Nielsen, S. O.; Lopez, C. F.; Srinivas, G.; Klein, M. L. *J. Phys.: Condens. Matter* **2004**, *16*, R481−R512.
(6) Safran, S. A. *Statistical Thermodynamics of Surfaces, Interfaces, and Membranes*; Addison-Wesley: Reading, MA, 1994.
(7) Boal, D. *Mechanics of the Cell*; Cambridge University Press: New York, 2002.
(8) Karatekin, E.; Sandre, O.; Hicham, G.; Borghi, N.; Puech, P.-H.; Brochard-Wyart, F. *Biophys. J.* **2003**, *84*, 1734−1749.
(9) Fromherz, P. *Chem. Phys. Lett.* **1983**, *94*, 259−266.
(10) van Dam, L.; Karlsson, G.; Edwards K. *Biochim. Biophys. Acta* **2004**, *1664*, 241−256.
(11) Vold, R. R.; Prosser, R. S. *J. Magn. Res. B* **1996**, *113*, 267−271.
(12) Luchette, P. A.; Vetman, T. N.; Prosser, R. S.; Hancock, R. E. W.; Nieh, M.-P.; Glinka, C. J.; Krueger, S.; Katsaras, J. *Biochim. Biophys. Acta* **2001**, *1513*, 83−94.
(13) Glover, K. J.; Whiles, J. A.; Wu, G.; Yu, N.; Deems, R.; Struppe, J. O.; Stark, R. E.; Komives, E. A.; Vold, R. R. *Biophys. J.* **2001**, *81*, 2163−2171.
(14) Sanders, C. R., II; Schwonek, J. P. *Biochemistry* **1992**, *31*, 8898−8905.
(15) Gaemers, S.; Bax, A. *Langmuir* **2001**, *123*, 12343−12352.
(16) Nieh, M.-P.; Glinka, C. J.; Krueger, S.; Prosser, R. S.; Katsaras, J. *Langmuir* **2001**, *17*, 2629.
(17) Rowe, B. A.; Neal, S. L. *J. Am. Chem. Soc.* **2003**, *19*, 2039−2048.
(18) Soong, R.; Macdonald, P. M. *Biophys. J.* **2005**, *88*, 255−268.
(19) Nieh, M.-P.; Raghunathan, V. A.; Glinka, C. J.; Harroun, T. A.; Pabst, G.; Katsaras, J. *Langmuir* **2004**, *20*, 7893−7897.
(20) Triba, M. N.; Warschawski, D. E.; Devaux, P. F. *Biophys. J.* **2005**, *88*, 1887−1901.
(21) Kozlov, M. M.; Lichtenberg, D.; Andelman, D. *J. Phys. Chem. B* **1997**, *101*, 6600−6606.

10.1021/la051278d CCC: $33.50
Published on Web 01/04/2006

dynamics simulation can address some questions about the structure of bicelles and systems with similar composition, but it faces some particular challenges when applied to mixed-amphiphile systems. The first challenge is simply one of equilibration: an accurate representation of the equilibrium segregation of two components into different microenvironments (e.g., the bilayer and its edge) requires adequate simulation times for the molecules to diffuse away from their initial positions. Even given time for satisfactory mixing within an aggregate, it is difficult to ensure that the aggregate size and composition are appropriate for each other; using the ideal bicelle model as an example, the selected mole fraction of DMPC determines the characteristic disk size. To predict the distribution of aggregate shapes, sizes, and compositions directly from a simulation would require that material for a statistically significant number of aggregates be included and sufficient time be allowed for equilibration not only of each aggregate but also of the transfer of material between aggregates. A multiscale approach is therefore appropriate, in which detailed model simulations are designed and analyzed to derive parameters for mesoscale modeling. In the present work, we simulate a coarse-grained molecular model to determine the degree of segregation and line tension in short-/long-chain lipid mixtures. Although the present model does not capture the vanishing or very low line tensions necessary to account for stable disks, ribbons, or pores observed experimentally in DMPC/DHPC mixtures—unlike the experimental behavior of C6 and C8 short-chain lipids the short-chain lipid in the present study remains stable as bilayers rather than reforming as globular or cylindrical micelles—it does shed some light on the structure and thermodynamics of the edges of mixed-lipid systems. In bilayers formed of predominantly the long-chain "L" component, a considerable excess of the short-chain "S" lipid at the bilayer edge and a corresponding reduction in line tension are observed. More surprisingly, in bilayers composed of predominantly short-chain lipids, there is an excess of L lipids near the edge as well and perhaps evidence for a slight decrease in line tension compared with a bilayer of pure S. This latter phenomenon can be understood only in light of a more detailed structure of the edge than has commonly been considered.

2. Methods

2.1. Force Field and Materials. The coarse-grained model of Marrink et al.[22] was used to represent two types of lipids and water in molecular dynamics simulations employing the GROMACS software package.[23] This model improves the speed of simulation by a factor of at least 10 over that of atomistic models by mapping four to six heavy atoms onto a single interaction site. It reproduces structural, elastic, and dynamic properties of dipalmitoyl phosphatidylcholine (DPPC) bilayers and is designed for use with short-ranged cutoffs on the electrostatic interactions. Recently, it was used to simulate domain formation in C20/C12 lipid mixtures in the context of the fluid- to solid-phase transition.[24] As mentioned above, the most commonly studied bicelle systems are mixtures of DMPC and DHPC, which have dual C14 and C6 alkyl tails, respectively. However, because the coarse-grained model maps four methylene groups to a single united atom, within the resolution of the model it is possible to represent alkyl chains with only length a multiple of four. We have selected the slightly longer (C16 tails) and widely studied DPPC molecule. The corresponding short-chain lipid with the same headgroup but with C8 tails (i.e., removal of two united atoms from each tail of DPPC) is called dicapryloyl phosphatidylcholine (DCPC). The long- and short-chain components will hereafter be denoted as L and S following ref 11.

Table 1. Synopsis of Simulation Runs[a]

ribbons						
%L	temp (K)	time (ns)	L	S	W	box (nm)
0	300, 323	400	0	966	15 900	17.4, 8.0, 20.4
20	300, 323	800	130	520	11 361	17.3, 8.0, 14.8
35	300, 323	800	228	422	11 361	17.7, 8.0, 14.8
50	300, 323	800	326	324	11 361	18.0, 8.0, 14.8
59	300, 323	800	566	400	15 900	18.8, 8.2, 20.0
73	300, 323	800	474	172	10 567	18.4, 8.4, 13.6
81	300, 323	800	482	112	11 604	19.0, 8.4, 13.6
85	300, 323	800	550	94	10 567	18.5, 8.5, 13.6
100	300, 323	2000	966	0	15 900	19.3, 8.3, 20.4

bicelles						
%L	temp (K)	time (ns)	L	S	W	box (nm)
48	300	100	458	487	58 475	24.8, 27.2, 11.9
58	300	144	553	392	58 095	24.8, 27.0, 12.0
74	300	112	698	247	57 515	24.8, 27.1, 11.9
85	300	132	804	142	57 095	24.9, 27.1, 11.9

assembly							
type	%L	temp (K)	time (ns)	L	S	W	box (nm)
random	74	323	212	699	247	38456	26.2, 26.3, 8.6
ran-disk	75	323	212	744	250	37000	24.8, 27.3, 8.5

[a] Listed are temperatures; run duration times scaled by a factor of 4; number of long-chain lipids L; number of short-chain lipids S; number of water united atoms W; and average *s*, *y*, *z* box dimensions.

2.2. Initialization. *2.2.1. Disks and Ribbons.* Our initial systems were made from an equilibrated 128 L (DPPC) bilayer configuration provided by Marrink. This rectangular patch was periodically duplicated into a 3 × 3 grid as needed. From this large bilayer, circular and ribbon-shaped patches were cut. In this and later stages of system preparation, care was taken to maintain a symmetric number of lipids in each bilayer leaflet. The void left from the removal of lipids was filled by randomly inserting water (using a hard-sphere overlap condition) until the box density was close to 1.0 g/mL. At this stage, lipids along the edges of the bilayer were converted to S by removing two united atoms from each tail. Unfavorable contacts in these systems were relaxed using steepest-descent energy minimization. The system densities relaxed quickly through coupling to a pressure reservoir during the simulations. The slowest equilibration mode involves the lateral lipid distribution. In assemblies of this size (∼10 nm), 100 to 200 ns was required to stabilize the rms distance of each species from the middle. Table 1 gives the number of lipids of each kind and number of water molecules in each system.

2.2.2. Assembly. Two additional simulations were performed that were aimed at understanding aggregate formation and evolution. In one system, a circular disk was cut from the bilayer as above, but instead of mutating the subset of lipids along the disk edge, lipids were randomly chosen from each leaflet for mutation. This resulted in a bicelle with a uniform distribution of large and small lipids throughout its radius. The other run started from a more random distribution of lipids. A single L configuration was stacked in three dimensions like blocks, and a random set of these were mutated to S. Finally, solvent molecules were randomly inserted up to a density of about 1.0 g/mL. The final density was determined by the fluctuation and relaxation of the cell volume determined by a pressure coupling of 1 bar.

(22) Marrink, S. J.; de Vries, A. H.; Mark, A. E. *J. Phys. Chem. B* **2004**, *108*, 750−760.
(23) Lindahl, E.; Hess, B.; van der Spoel, D. *J. Mol. Model.* **2001**, *7*, 306−317.
(24) Faller, R.; Marrink, S. J. *Langmuir* **2004**, *20*, 7686−7693.

2.3. Dynamic Algorithm. The details of the methods for propagating the Hamiltonian equations of motion were similar to those used in ref 22. Velocity and volume rescalings as prescribed by the Berendsen algorithm were used to maintain the desired temperature and pressure. In the ribbon simulations, the box length in the direction parallel to the ribbon edges was fixed, whereas the orthogonal directions were coupled jointly to a pressure of 1 bar. In the disk simulations, the box length parallel to the initial disk axis was coupled to 1 bar, and the orthogonal directions were coupled jointly to the same pressure ("semi-isotropic coupling"). In other words, the constraints were $NP_{xy}L_zT$ and $NP_{xy}P_zT$ for the ribbons and disks, respectively.

Table 1 summarizes the salient aspects of the molecular dynamics runs, which were carried out at two temperatures: 300 and 323 K. Whereas DPPC has a solid−fluid transition temperature of 314 K,[25] the coarse-grained model exhibits a lower transition temperature; therefore, both of the temperatures in this study correspond to fluid-phase bilayers. The duration of the simulations ranged from 100 ns to 2 μs. Marrink et al.[22] have recommended that times be rescaled by a factor of 4 to correct the dynamic artifact of the coarse graining (smoother structures). Therefore, our times and derivatives thereof such as the diffusion coefficients are all reported with the use of this scaling factor.

2.4. Analysis. The structural features (e.g., density profiles) of the disks and ribbons were analyzed with respect to internal coordinates, similarly to that in ref 26. Both types of structures contained roughly flat bilayer regions with (on average) uniform composition, which were designated "bulk" regions, surrounded by curved-edge regions. For ribbons, the z axis was defined to be parallel to the edge of the box in the direction of the bilayer edge. The projection of the lipid coordinates onto the plane normal to the z axis was then used to determine the principle components of the 2-D inertial tensor of the bilayer cross section for each instantaneous structure analyzed. The component normal to the bilayer interior was designated the y axis, and the component directed from edge to edge was designated the x direction. Density profiles of both lipid types along the x axis of ribbons were obtained in terms of atoms per unit projected surface area. Within the central strip of the ribbon, from $x = -3$ to $+3$ nm, the composition and structure were uniform enough to designate as "bulk"-like. Area per headgroup of this bulk region was calculated by integrating the number of lipids in this region and dividing by twice its area. As a test for finite size effects, a wider ribbon containing 50% more lipids (20% L, 80% S) showed essentially the same structure, distribution, and line tension as the standard-width ribbon with the same bulk composition (data not shown). For disks, the principle components of the inertial tensor at each time step are determined, and the one normal to the bilayer plane is designated the z axis; all structural determinations were made radially from this axis. For calculations of bulk properties, averages were taken over the cylindrical core of radius 3 nm from the inertial z axis.

The line tension along the edge of the ribbons was expressed from below

$$\Lambda = \frac{1}{2}\left\langle L_x L_y \left[\frac{P_{xx} + P_{yy}}{2} - P_{zz}\right]\right\rangle \qquad (1)$$

where the factor of $^1/_2$ accounts for the presence of two edges in the ribbon, L_x and L_y are box dimensions, and P_{xx}, P_{yy}, and P_{zz} are the diagonal components of the instantaneous pressure tensor. Line tension, the free-energy cost to extend the ribbon edge per unit length, is effectively obtained from the force required to extend the z dimension of the simulation box (i.e., $-P_{zz}(L_xL_y)$) by subtracting the component of that force arising from the bulk pressure, taken as the average of P_{xx} and P_{yy}. The surface tension is assumed to be zero because the bilayer area is not constrained in these simulations. For details, please refer to ref 26.

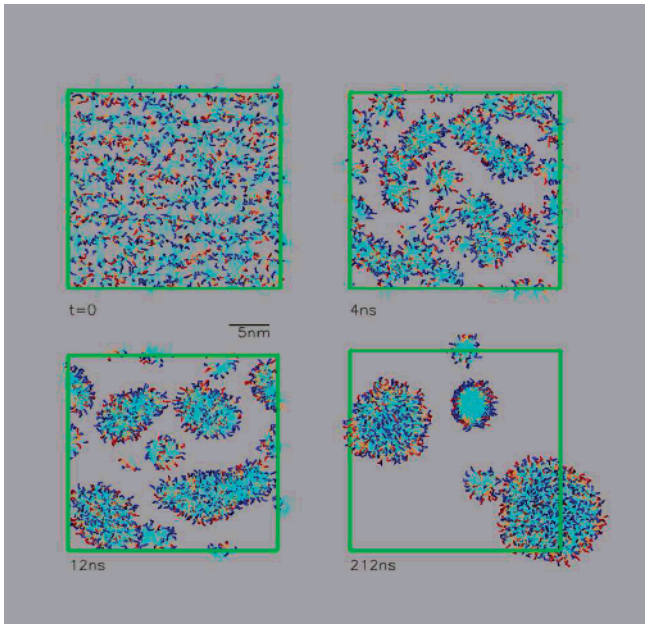

Figure 1. Snapshots during the course of the assembly run. Lipid types are distinguished by headgroup color: L, blue; S, red. The solvent is omitted from view. In the final snapshot, some lipids are represented in neighboring image cells to illustrate the continuity of the aggregates.

Table 2. Aggregate Properties after 212 ns of the Assembly Run[a]

morphology	lipids	%L	R_{gyr}	R_T	T
disk	464	76	4.8	4.4	4.3
disk	290	70	3.9	2.8	4.3
cylinder	135	77	3.2		
sphere	32	66	1.7		
sphere	25	76	1.6		

[a] T is the phosphate-based thickness of the disk interior, and R_T is the radius corresponding to the drop in thickness at the edge.

3. Results

3.1. Dynamics. *3.1.1. Assembly.* Snapshots from the assembly run, beginning from a random distribution of lipids and water, are shown in Figure 1. Small micelles form quickly. After the first 20 ns, the aggregates evolve more slowly with the occasional fusion of smaller aggregates into larger ones. After 212 ns, the system is composed of two large disklike micelles, a cylindrical micelle of "infinite" length (because of periodic boundaries), and two small spherical/irregular micelles. The bicelles show a strong rise in S density approaching the edges. The aggregate compositions and sizes are described in Table 2.

To establish whether the segregation was an equilibrium phenomenon, in a separate 200 ns simulation a bicelle disk of radius ∼15 nm, initiated with a random distribution of L and S lipids, was observed to undergo partial segregation of the S component to the edge. The distribution of lipids stabilized after 160 ns, as assessed from stationary density profiles and rms radial coordinates of each species. The disk shape of the bicelle is flexible, going through visible perimeter and out-of-plane

(25) Lewis, R. N. A. H.; McElhaney, R. N. In *The Structure of Biological Membranes*; Yeagle, P., Ed.; CRC Press: Boca Raton, FL, 1992; Chapter 2.
(26) Jiang, F. Y.; Bouret, Y.; Kindt, J. T. *Biophys. J.* **2004**, *87*, 189−192.

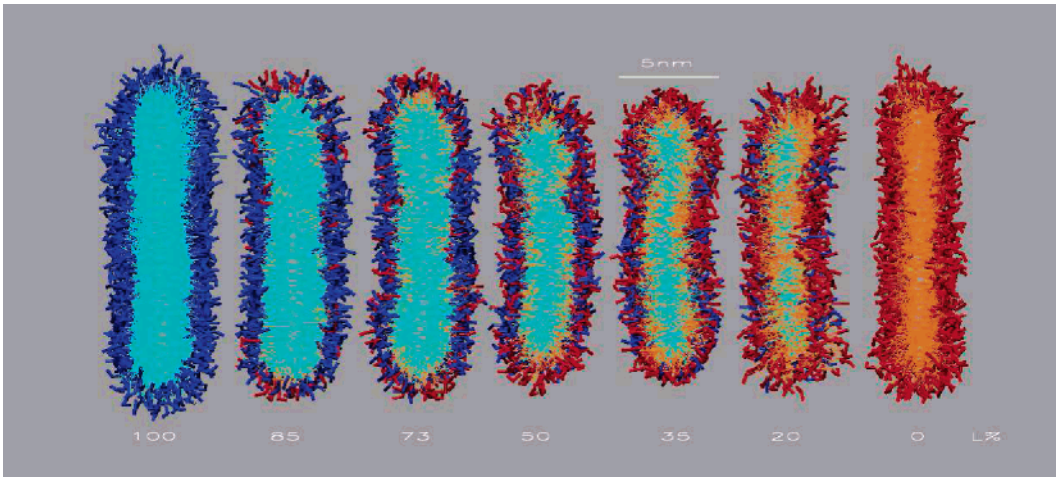

Figure 2. Snapshots from ends of ribbon simulation at compositions from 0 to 100% L at 323 K. A cross section of depth 40 nm is shown: S, red; L, blue.

fluctuations. Subsequent simulations were initiated with S lipids positioned at the bilayer rim to reduce the necessary equilibration time. Simulations performed on both disks and ribbons showed few substantive differences; because the ribbon geometry[26,27] allows direct measurement of the line tension, smaller system sizes, and easier interpretation, our analysis focuses mostly on the ribbon runs. The effect of the different local curvatures exhibited in disk, ribbon, and pore edges is unknown. The ribbon geometry has the advantage of having the same local edge curvature regardless of size (unlike disks that have radius-dependent planar curvature and pores that have variable negative planar curvature and also negative transverse curvature).

3.2. Structure. *3.2.1. Bulk-Edge Equilibrium.* As in an experiment, each simulation starts by selecting the overall mole fractions of L and S. Experiments provide indirect evidence for partitioning of S to the edges, and the ideal bicelle model proposes an essentially perfect partitioning of the two species. Here we consider bicelles and ribbons to consist of two zones in chemical equilibrium. The definition of the bulk region is unambiguous. Our assemblies all exhibit a region of constant bilayer-like properties (e.g., thickness, S- and L-atom densities). Throughout, we use the bulk mole fraction of L, $n_{b,\mathrm{L}}$, as the independent variable (in favor of the total mole fraction). It is calculated from atom density profiles $\rho_{\mathrm{L}}(x)$ and $\rho_{\mathrm{S}}(x)$ using

$$n_{b,\mathrm{L}} = \frac{\int_b (\rho_{\mathrm{L}}/12)\,\mathrm{d}x}{\int_b \mathrm{d}x\,\{(\rho_{\mathrm{S}}/8) + (\rho_{\mathrm{L}}/12)\}}$$

where the bulk region is taken as the central 3 nm for all ribbons and 12 and 8 are the number of united atoms in L and S molecules, respectively.

3.2.2. Composition Profile. Composition profiles were computed as a function of the distance from the aggregate center toward the edge. These are presented for the ribbons, in terms the mole fraction of S, at 300 and 323 K in Figure 3, labeled by %L lipid in each ribbon. The partitioning S to the edge is apparent in all profiles. It is clear that segregation is not absolute for this pair of lipids because considerable S densities are retained in the middle. The bicelle radial mole fraction profiles (not shown) are similar, though with apparently greater segregation (perhaps not fully equilibrated). A depletion minimum in the S mole fractions is also observed near each edge. This feature is most pronounced

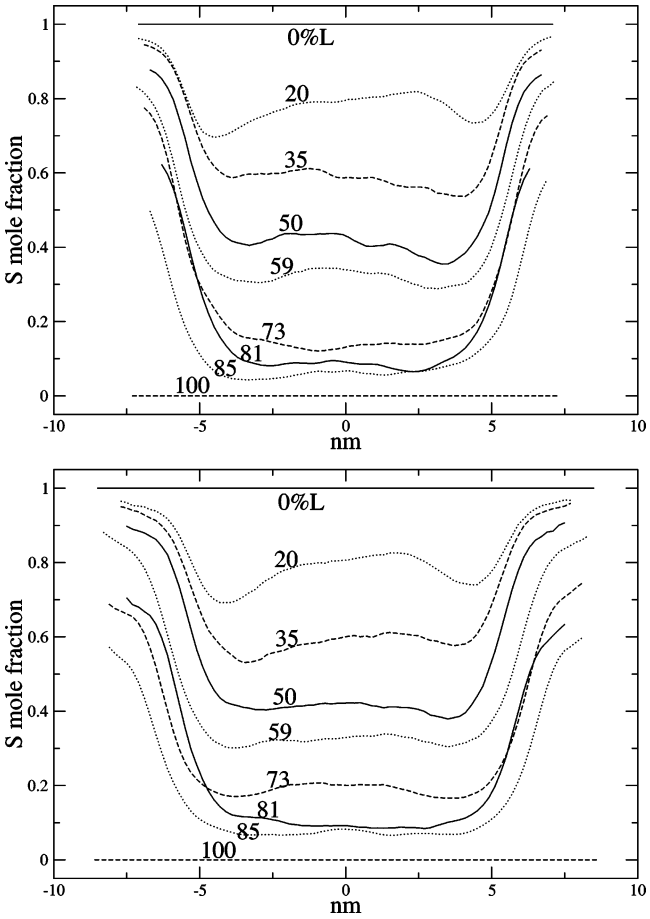

Figure 3. Mole fraction of S vs position in ribbons at 300 K (top) and 323 K (bottom).

when the system is rich in S but appears to be a general, reproducible, equilibrium property of the mixed-bilayer edge.

3.2.3. Thickness. Figure 4 shows the thickness profiles of ribbons at 300 and 323 K. Those bulk regions with a high percentage of S have a smaller thickness due to the decrease in average molecule length. A bulge in the membrane near the edge is seen, as was earlier observed in atomistic simulations of a DMPC bilayer ribbon,[26] but is more pronounced by as much as 10% of the bulk thickness for L-minority ribbons.

3.2.4. Area per Headgroup. The area per headgroup (well defined only in the bulk) is one measure that showed a consistent

(27) Kasson, P. M.; Pande, V. S. *Biophys. J.* **2004**, *86*, 3744−3749.

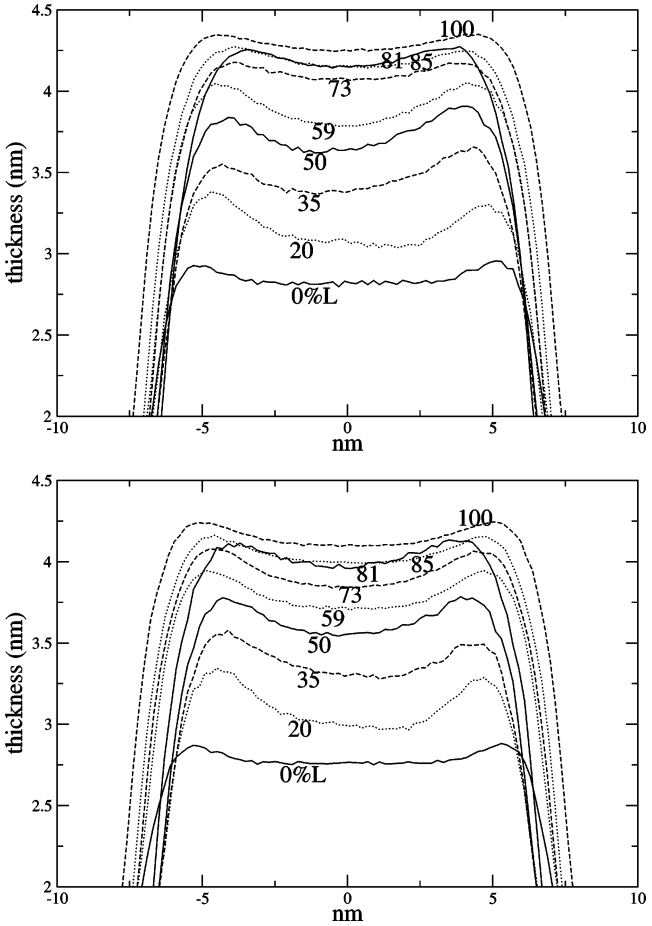

Figure 4. Bilayer thickness vs position in ribbons at 300 K (top) and 323 K (bottom).

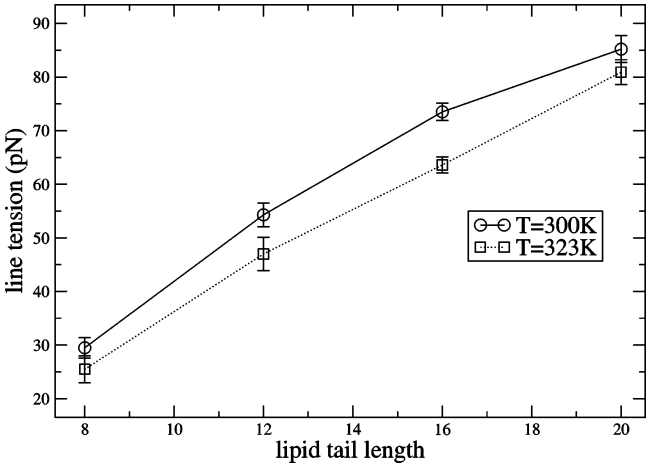

Figure 5. Line tension of pure component ribbons as a function of lipid tail length (number of carbons per tail).

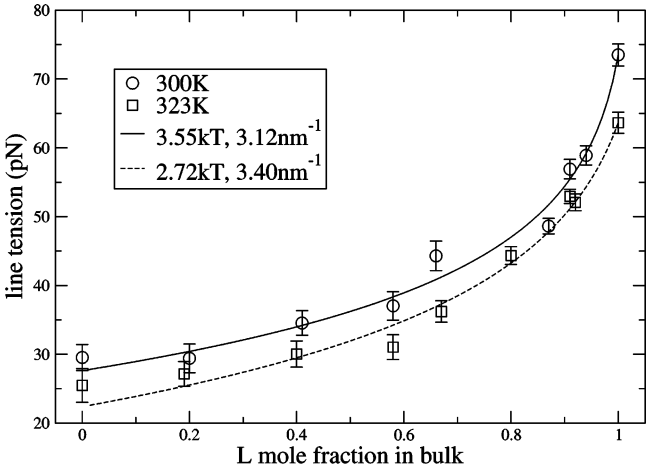

Figure 6. Line tension of ribbons vs bulk composition (mole fraction of L) at 300 and 323 K. The two-parameter curve fits are explained in the Discussion section.

difference between ribbon and disk simulations. The area per headgroup over a range of compositions was consistently ~0.01 nm^2 higher for the ribbons than for the disks. This difference, although small, may indicate disk squeezing.

3.3. Line Tension. The ribbon simulations provide a convenient means to measure the line tension along bilayer edge. The ensemble chosen, $NP_{xy}L_zT$, allows the area of the bilayer to change but causes the length of the ribbon to be constant. Therefore, the excess (negative) pressure in the edge direction is proportional to the contraction force along the ribbon's edge. (A more indirect method[22] has been used on bilayer pores using a simple thermodynamic model.)

To provide context, we first performed simulations of single-component bilayer ribbons composed of lipids with C8, C12, C16, and C20 tails (C8 = S and C16 = L). The results in Figure 5 show that decreasing the tail lengths produces a roughly linear decrease in line tension at the edges. A comparison of the temperatures indicates a "softening" of the line tension on heating from 300 to 323 K (within the fluid phase). The error bars are computed from the estimator $\sqrt{s^2/n}$ where s^2 is the sample variance and n is the number of *independent* samples obtained from block averaging. For the mixed S/L bilayer ribbons, the line tension as a function of the bulk mole fraction of L is shown in Figure 6. The bulk is considered to be the interior of the bilayer aggregate where the edge influence is minimal; therefore, the properties of a normal bilayer are recovered. For an isolated bicelle or ribbon, it is useful to think of the edge and bulk as two distinct regions that are in chemical equilibrium; therefore, the specification of the bulk composition determines the system. Alternatively, one could specify the total composition or the edge composition, but the former is size- and geometry-dependent and the latter as we shall see is less well defined. The line tension is observed to decrease with increasing temperature and decreasing mole fraction of L. At a bulk mole fraction of <0.6, the line tension decay becomes considerably flatter.

3.4. Lattice Model. Suppose we have a lattice composed of M_b bulk sites and M_e edge sites, each of which must be filled by either an L or an S particle. If ϵ_L and ϵ_S represent the energy costs to place long and short lipids, respectively, in an edge environment, then the total edge energy is $E = M_e(\epsilon_L - n_{e,S}\Delta\epsilon)$, with $\Delta\epsilon = \epsilon_L - \epsilon_S$ and $n_{e,S}$ being the mole fraction of S lipid in edge sites. The free energies of the bulk and edge are, in the thermodynamic limit, $k_BTM_b(n_{b,S}\ln n_{b,S} + n_{b,L}\ln n_{b,L})$ and k_BTM_e-$(n_{e,S}\ln n_{e,S} + n_{e,L}\ln n_{e,L}) + E$, respectively. Minimizing the total free energy of the system relates the equilibrium compositions of the edge and the bulk to the edge energy difference $\Delta\epsilon$:

$$\frac{n_{e,S}}{1-n_{e,S}} = \frac{n_{b,S}}{1-n_{b,S}}e^{\Delta\epsilon/k_BT} \tag{2}$$

The line tension associated with the model is found by differentiating the free energy with respect to the edge length M_el_e, where l_e is the length of one edge lattice site. At equilibrium,

$$\Lambda = l_e^{-1}\left(\Delta\epsilon + \ln\frac{n_{e,L}}{n_{b,L}}\right) \tag{3}$$

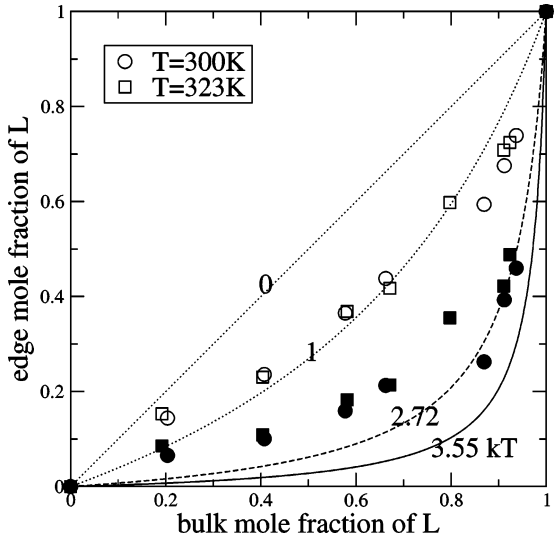

Figure 7. Bulk vs edge composition for density-based (open symbols) and thickness-based (solid symbols) defintions of the edge region. The curves are independent of this definition and correspond to those fit to the line tensions above at each temperature. The $\Delta\epsilon/k_BT = 0$ and 1 curves are shown only as points of reference.

To compare the results of this model to the simulation results, $\Delta\epsilon/l_e$ was constrained to equal the line tension of the pure L ribbon, whereas and l_e and $\Delta\epsilon$ were chosen to give the best least-squares fit of line tension versus bulk mole fraction of L at each temperature. The resulting values correspond to a linear density near 3 lipids/nm and $\Delta\epsilon \approx 3k_BT$ at both 300 and 323 K.

3.5. Edge Composition. In contrast to the definition of bulk composition, the definition of edge composition is more ambiguous because the composition varies significantly with the choice of edge boundary. We tried two definitions for the boundary of the edge: the point at which the thickness of the bilayer begins to taper and form the hemicylindrical edge, and the maximum in the peak of S lipid density. The former, due to the bulge at the ribbon edges, is taken simply as the location of the thickness peak. (Interestingly, the bicelles as studied do not have this bulge.) The lattice model parameters ($\Delta\epsilon$, l_e) from the line tension fit were used to predict the edge composition as a function of bulk composition. As seen in Figure 7, fair agreement is obtained for systems rich in L lipid when the edge boundary is defined from the S-density maximum but not when the edge boundary is placed at the thickness maximum. The temperature plays only a minor role in determining the distribution of lipids between the edge and bulk regions.

An unambiguous measure of the excess S lipid at the ribbon edge can be obtained using the Gibbs construction. The Gibbs adsorption isotherm is commonly used to describe the thermodynamics of interfaces such as the interface between bulk phases of oil and water. On a molecular scale, this interface is not sharp and has nonzero smoothly varying densities of oil and water. The Gibbs choice for the plane dividing two such phases fixes the excess "solvent" at zero. Other excess interfacial properties may then be defined with respect to this surface. In our adaptation of the Gibbs adsorption isotherm, we consider L to be the solvent and S to be the solute and the 1-D interface produced when their densities are projected onto the plane parallel to the bilayer. Of paramount interest is the excess S per unit length of the edge, which is plotted in Figure 9 and is shaped like the letter Π; the left branch is another manifestion of the depletion of L in the bulk already mentioned. In Table 3, the ribbon widths W_G from this analysis are also given.

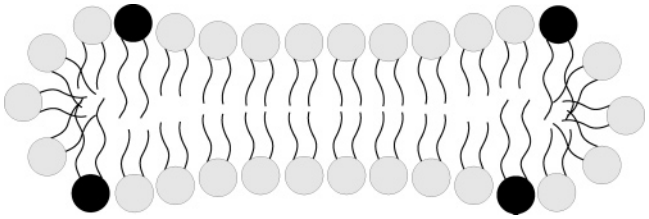

Figure 8. Idealized edge structure in the limit of low L.

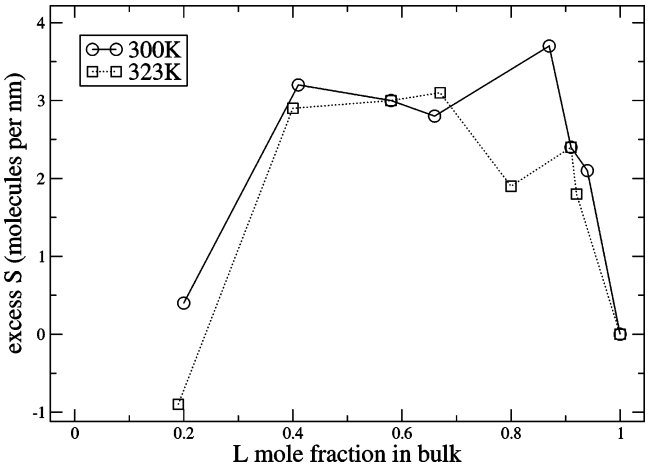

Figure 9. Excess S molecules found at the edge of ribbons vs bulk composition.

Table 3. Ribbon Properties[a]

%L	%Lb	A_b (nm^2)	T_b (nm)	W_T (nm)	W_G (nm)	XS (nm^{-1})	10^7D_L (cm^2/s)	10^7D_S (cm^2/s)
				300 K				
0	0	0.585	2.8	10.4	NA	NA	NA	3.9
20	20	0.592	3.1	9.6	13.7	0.4	2.2	3.3
35	41	0.587	3.4	8.6	11.6	3.2	2.1	3.1
50	58	0.586	3.6	8.2	11.7	3.0	1.8	2.7
59	66	0.584	3.8	8.7	12.4	2.8	1.8	3.0
73	87	0.585	4.1	7.4	11.7	3.7	2.5	4.0
81	91	0.584	4.2	7.3	11.3	2.4	1.7	2.7
85	94	0.589	4.2	8.2	12.7	2.1	2.0	2.9
100	100	0.593	4.3	8.6	14.0	0.0	1.9	NA
				323 K				
0	0	0.614	2.8	10.6	NA	NA	NA	5.6
20	19	0.619	3.0	9.2	14.2	−0.9	3.6	4.6
35	40	0.616	3.3	8.8	11.7	2.9	2.8	4.4
50	58	0.616	3.6	8.2	11.7	3.0	2.2	4.1
59	67	0.613	3.7	9.6	12.9	3.1	2.7	3.8
73	80	0.619	3.9	9.1	13.5	1.9	2.2	3.5
81	91	0.621	4.0	7.2	12.1	2.4	2.2	3.9
85	92	0.625	4.0	9.4	13.7	1.8	2.5	3.5
100	100	0.631	4.1	10.1	14.9	0.0	2.7	NA

[a] The bulk "b" region denotes the central 3 nm of each ribbon. Thus, %Lb, A_b, and T_b are the percent L, lipid area, and thickness in the bulk region, respectively. The width W_T is the distance between peaks of the thickness profile, and the width W_G is the distance between Gibbs surfaces. The excess S on the edge, XS, is given in terms of molecules per unit edge length. The lateral diffusion coefficients are given by D_L and D_S in units of 10^{-7} cm^2/s (scaled time).

4. Discussion

Self-assembly from a starting point of randomly mixed long-chain (L) and short-chain (S) lipids in solvent led to a preponderance (78%) of lipids in disklike aggregates, characterized by a relatively flat bilayer center rich in the L component encircled by a hemicylindrical rim enriched in the S component. Given the short time allowed for equilibration and the influences of the box size and shape, these results are suggestive only of

the true equilibrium statistics of the system. What they indicate, however, is that the mixing of long- and short-tailed phospholipids does tend to produce disklike rather than spherical or cylindrical micelles. Because of the periodic boundary conditions, the cylindrical micelle was able to form without high-energy end caps across the narrowest box dimension (8.6 nm). The exchange of lipids between aggregates did not occur during the simulation, so the distribution of L and S lipids among the aggregates and the aggregate distribution itself have probably not reached equilibrium. Nonetheless, it is interesting that the cylindrical micelle has the highest fraction of L. Partitioning of S lipids to the edge is apparent in both disk structures.

The process of edge segregation was also observed over a period of 200 ns in a separate simulation, starting from a uniform lateral distribution within a 15 nm diameter bilayer disk, and confirms that the segregation is an equilibrium effect and not an artifact of the initial assembly kinetics. In the pure L (DPPC) bilayer ribbon at 323 K, we find a lateral diffusion constant of 2.7×10^{-7} cm^2/s, in agreement with the previous report of 3×10^{-7} cm^2/s for this model.[22] (We did not distinguish between edge or bulk diffusion in the coefficients reported here. That seems to make little difference because the 20% L ribbon had nearly the same D_S when its width was increased by 50%.) The S lipid has somewhat higher mobility by $\sim 1 \times 10^{-7}$ over the whole range of mole fractions; the diffusion constants of both components increase as the composition is shifted toward a pure S bilayer. At a lower temperature of 300 K, diffusion constants are smaller and follow similar trends. The enhancement of S at the edge is significant. Its mole fraction at the edge is as much as 4 to 6 times that in the bulk. Even when a third of the bulk molecules are S lipids, their mole fraction at the edge nearly doubles. The excess appears to reach a saturation point when the bulk is ~87% L (300 K), from which point further replacement of L with S mostly adds to the concentration of S in the bulk (Figure 3). On thermodynamic grounds, the partial segregation of S lipids toward the bilayer edge implies that their presence reduces the line tension. We have confirmed and quantified this effect by monitoring the decreasing pressure anisotropy in mixed-lipid bilayer ribbons. In contrast to the known experimental behavior of C6- and C8-tail phosphatidylcholines (which self-assemble into spherical, elliptical, or cylindrical micelles[29]), the coarse-grained S lipids used in this study self-assemble predominantly into bilayers and have a nonvanishing line tension. The fact that the addition of S lipids to the L bilayer lowers the system line tension, but does not eliminate it, would seem to be at variance with the observations that the addition of DHPC to DMPC bilayers can produce stable disks, ribbons, and pores.[10,19,20] Thus, if one assumes that the model for S used here does not represent DHPC well enough, namely, underestimating its ability to confer edge stability, then it follows that it also underestimates the degree of segregation. (Actually, we recently learned of a modification[28] to the force field used here meant to improve the line tension. We performed several tests on this new version to determine its effect on the line tension in our mixed systems. In one case (~60% L), the line tension is reduced considerably but does not vanish. To eliminate the line tension completely, one has to replace S with its smaller C4-tail analogue. Thus, the conclusions given here about a C8-tail lipid (S) are not entirely appropriate for application to the experimental C6-tail lipids, which cannot be modeled in this force field.) However, recent experiments agree with our results that the two components are not entirely segregated,[10,20] which leads to nontrivial effects.

It is not surprising to find a positive excess of S lipids at the edge in bilayers rich in L; however, the negative edge excess of S seen in bilayers composed predominantly of S was entirely new. This counterintuitive result, that a long-chain lipid can behave as an edgactant in a bilayer of shorter-chain lipids, can be understood in terms of the bilayer thickness profile near the rim. A peak in the L lipid density, and in the mole fraction of L lipids, is seen over the full range of mixture compositions to coincide approximately with the thickness maximum of the bilayer. The bulging of the bilayer near the edge, which is also seen in atomistic simulations of a pure DMPC bilayer,[26] reduces the curvature experienced by lipids further out on the rim. As the proportion of S is increased and the interior bilayer consequently thins, L lipids are retained mainly near the rim and augment the bulge. This is only natural because there is no advantage for them to be located in the predominantly S bilayer while near the edge they help prevent an increase in curvature required to form the rim. It is natural that the long-chain lipid will tend to concentrate in the thickest region of the bilayer, as represented by the cartoon in Figure 8. By analogy to the Gibbs adsorption isotherm,[30] the excess of L lipids near the edge implies that increasing L concentration will tend to lower the line tension in this concentration regime and that therefore the proportion of S that gives the lowest line tension will be less than 100%. In the present simulation, the line tensions of systems with 80 and 60% bulk S were statistically indistinguishable from the line tension with 100% S, so if there is a minimum, it should be rather shallow. Nonetheless, the results suggest that some important phenomena may be missed when the bilayer edge is modeled as a simple hemicylindrical cap fused onto a flat bilayer, as is common in phenomenological models.[21]

It is useful to determine how well a very simple model can account for the general trends despite these complexities. The statistical lattice model deployed here has what another simple model, the ideal bicelle, does not—mixing entropy (of the form $n \log n$).[21] However, it makes several important assumptions: (1) that there is a clear-cut distinction between edge and interior sites, (2) that S and L lipids occupy the same area at the edge, and (3) that the preference of S lipids for the edge does not change as the bulk composition changes. Violation of the third point is actually fairly subtle; the "two-dimensionality" of the lattice model could not have foreseen the impact of the thickness on edge energy and could account for it only through an ad hoc variation of $\Delta\epsilon$. Even though we can see all of these assumptions violated in the simulations, we find that the model qualitatively can fit the dependence of line tension on bulk composition. For the edge composition, fair agreement is seen for systems rich in L lipids when the edge boundary is defined as the S-density maximum but not when the edge boundary is placed at the thickness maximum. For systems rich in S, the edge region has a greater L population well above that predicted by the lattice theory, owing largely to the L concentration near the bulge as discussed above.

4.1. Bicelle Squeezing. Comparing data from Tables 3 and 4, we observe consistently smaller areas per lipid headgroup, determined within the central bulk bilayer region as defined in section 2.4, in disk simulations than in ribbon simulations. The line tension of a bilayer disk may lead to distortions of the bilayer structure to reduce the perimeter. One mode of distortion is bending of the bilayer, which for large enough disks will ultimately

(28) Marrink, S. J.; Mark, A. E. *Biophys. J.* **2004**, *87*, 3894−3900.

(29) Tausk, R. J. M.; van Esch, J.; Karmiggelt, J.; Voordouw, G.; Overbeek, J. T. G. *Biophys. Chem.* **1974**, *1*, 184−203. Tausk, R. J. M.; Oudshoorn, C.; Overbeek, J. T. G. *Biophys. Chem.* **1974**, *2*, 53−63.

(30) Chandler, D. *Introduction to Modern Statistical Mechanics*; Oxford University Press: New York, 1987.

Table 4. Disk Properties[a]

%L	%Lb	A_b (nm^2)	T_b (nm)	R_T (nm)
48	93	0.579	4.2	6.8
58	95	0.579	4.2	6.6
74	99	0.576	4.3	6.8
85	100	0.573	4.4	7.2

[a] Same as for Table 3, where R_T is the radial equivalent to W_T.

lead to vesicle formation but for small disks is confined to fluctuations from the flat disk into slightly cupped structures.[9] Another mode of distortion is the lateral compression of lipids, accompanied by an increase in bilayer thickness to maintain a constant lipid volume. Quantitatively, an inward surface pressure, analogous to the Laplace pressure difference across a curved 2-D interface,[6] is expected with a magnitude of Λ/R, which is equal and opposite to the surface tension arising from a circular pore of radius R.[31] At line tension $\Lambda = 7 \times 10^{-11}$ N and disk radius $R = 7 \times 10^{-9}$ m, this surface pressure is around 0.01 N/m. Dividing the pressure by the previously published[22] value for the area compressibility modulus of a small lipid patch ($K_A = 0.40$ M/m) yields a dimensionless area strain of 0.025, consistent with the roughly 0.01−0.02 nm^2 per headgroup reduction.

5. Conclusions

We have performed molecular dynamics simulations of aqueous bidisperse homologous phospholipids. The lipids were coarse grained[22] to about 4 atoms per interaction site in order to expand the range of system size and simulation time, and one of the lipid species was given short-chain tail groups with the expectation that it was to promote bilayer edge formation. From three different starting points—a random mixture, a random bicelle, and a segregated bicelle—we found that the lipid mixture either formed or remained in these disklike aggregates. Moreover, the disks exhibited essentially the same lateral distribution of lipids with a strong, but far from complete (as suggested by the ideal bicelle model), segregation of the short-chain lipids to the edge. The line tension around the rim of the bicelles squeezes them, causing a discernible increase in thickness relative to continuous or ribbon bilayers. Simulations of single ribbon-shaped aggregates proved to be the most convenient and systematic approach to isolate the properties of mixed-lipid edges. Adding small amounts of short-chain lipids produces a strong decrease in line tension, as does, to a lesser extent, increases in temperature. The change in line tension flattens as the two species become equally populous. A novel effect occurs in the not widely studied regime when the aggregate consists mainly of short-tail lipids. Rather than being located preferentially in the bulk bilayer interior, the long-chain lipids are retained predominantly near the edge in order to reduce the cap's curvature energy. This work sheds some light on the complexity in bilayer edges that is missed by reductionist modeling. For example, the assumption of complete segregation is demonstrated here to be a poor approximation. The reason for incomplete segregation is explained well by a simple lattice model that incorporates an entropic mixing term in addition to the energy of the edge.

Acknowledgment. This material is based upon work supported by the National Science Foundation under grant CHE-0316076.

LA051278D

(31) Leontiadou, H.; Mark, A. E.; Marrink, S. J. *Biophys. J.* **2004**, *86*, 2156−2164.